Applied Catalysis B: Environmental 238 (2018) 454–464

Contents lists available at ScienceDirect

Applied Catalysis B: Environmental

journal homepage: www.elsevier.com/locate/apcatb

Platinum/polypyrrole-carbon electrocatalysts for direct borohydride-peroxide fuel cells

Raisa C.P. Oliveira[a,1], Jadranka Milikić[b,1], Elif Daş[c], Ayşe B. Yurtcan[c,d], Diogo M.F. Santos[a,*], Biljana Šljukić[a,b,*]

[a] CeFEMA, Instituto Superior Técnico, Universidade de Lisboa, 1049-001 Lisbon, Portugal
[b] Faculty of Physical Chemistry, University of Belgrade, Studentski trg 12-16, Belgrade, Serbia
[c] Department of Nanoscience and Nanoengineering, Atatürk University, Erzurum, Turkey
[d] Department of Chemical Engineering, Atatürk University, Erzurum, Turkey

ARTICLE INFO

Keywords:
Platinum
Polypyrrole-carbon composite
Borohydride oxidation reaction
Hydrogen peroxide reduction reaction
Direct borohydride fuel cell

ABSTRACT

Polypyrrole-carbon (PPy-C) composites having different amounts of carbon (5–35 wt.%) decorated with platinum nanoparticles (Pt/PPy-C) were prepared and investigated for borohydride oxidation reaction (BOR) in alkaline medium and for hydrogen peroxide reduction reaction (HPRR) in acidic medium. Structural and morphological properties and composition of these electrocatalysts were determined by FTIR, Raman, XPS, SEM/EDS, TEM and ICP-MS analyses. Pt/PPy-C electrocatalysts were evaluated for BOR and HPRR by cyclic voltammetry and chronoamperometry. Faradaic and kinetic parameters, such as the number of exchanged electrons, n, charge transfer coefficient, α, apparent activation energy, E_a^{app}, and order of reaction, β, were calculated. n for BOR ranged from 6.0 to 7.6, while n for HPRR ranged from 1.0 to 2.0. E_a^{app} was found to range from 10 to 18 kJ mol^{-1} for BOR and from 8 to 14 kJ mol^{-1} for HPRR. The BOR was found to be a 1st order reaction with respect to BH_4^-. Pt/PPy-$C_{35\%}$ electrocatalyst showed the best activity for both reactions. Fuel cell tests were done with Pt/PPy-C electrodes as anode, as cathode and as both anode and cathode in a direct borohydride-peroxide fuel cell (DBPFC). DBPFC with Pt/PPy-$C_{35\%}$ as anode electrocatalyst gave the highest peak power density of 1432 W g_{Pt}^{-1} at current density of 2046 A g_{Pt}^{-1} and cell voltage of 0.70 V.

1. Introduction

The use of direct borohydride fuel cells (DBFCs) and direct borohydride-peroxide fuel cells (DBPFCs) as power sources has several advantages: they have high theoretical cell voltage (1.64 V in case of DBFCs or 2.11–3.02 V in case of DBPFCs); high energy density (9.3 kWh kg^{-1}); and, finally, no CO poisoning during their operation [1–4]. Recent studies related to DBFCs/DBPFCs are mostly focused on finding appropriate anode materials that are both economic and highly efficient for borohydride oxidation reaction (BOR) [5–12].

Oxidation of sodium borohydride ($NaBH_4$) as a fuel is an eight-electron process in highly alkaline conditions (Eq. (1)), with its mechanism being still under discussion [1–4,13,14]

$$BH_4^- + 8\,OH^- \rightarrow B(OH)_4^- + 4H_2O + 8e^- \quad E^0 = -1.24\,V \text{ vs. SHE} \qquad (1)$$

A major issue is borohydride (BH_4^-) hydrolysis reaction proceeding in parallel with its oxidation, leading to decrease of cell performance. During BH_4^- partial hydrolysis, hydrogen (H_2) and hydroxyborohydride ion (BH_3OH^-) are released (Eq. (2)) [1–3,13–16].

$$BH_4^- + H_2O \rightarrow H_2 + BH_3OH^- \qquad (2)$$

Thus, depending on the choice of anode material, BOR is given by Eq. (3) [1–3,7,8],

$$BH_4^- + x\,OH^- \rightarrow B(OH)_4^- + (x-2)\,H_2O + (4 - x/2)\,H_2 + x\,e^- \qquad (3)$$

where x is the actual number of exchanged electrons [17]. Among different materials investigated for BOR [1–3,13,14], gold (Au) has been previously suggested to lead to the highest faradaic efficiency, while platinum (Pt) has been suggested to lead to higher BOR rates, but also to significant BH_4^- hydrolysis [6,8,18–21]. Recent studies also point out palladium (Pd) as a promising anode material for DBFCs [7,22,23]. Namely, Pd activity for BOR was found to be maintained at high $NaBH_4$ concentrations corresponding to DBFC operating

* Corresponding author at: CeFEMA, Instituto Superior Técnico, Universidade de Lisboa, 1049-001 Lisbon, Portugal.
E-mail addresses: diogosantos@tecnico.ulisboa.pt (D.M.F. Santos), biljana.paunkovic@tecnico.ulisboa.pt (B. Šljukić).
[1] Equally contributed.

https://doi.org/10.1016/j.apcatb.2018.06.057
Received 21 February 2018; Received in revised form 15 June 2018; Accepted 22 June 2018
Available online 23 June 2018

conditions [22].

Cathodic reaction in DBFCs is either oxygen (O_2) or hydrogen peroxide (H_2O_2) reduction reaction (HPRR), which in acidic media is given by Eq. (4) (the so-called direct HPRR mechanism) [24–26].

$$H_2O_2 + 2H^+ + 2e^- \rightarrow 2\,H_2O \quad E^0 = 1.78\ \text{V vs. SHE} \tag{4}$$

Use of H_2O_2 as oxidant has several advantages including the above mentioned higher cell voltage compared to that of cell with O_2 as the oxidant. Still, its spontaneous chemical decomposition to water and O_2 (Eq. (5)) in the presence of some metals or at higher temperatures presents main disadvantage [24,27].

$$H_2O_2 \rightarrow H_2O + \frac{1}{2}O_2 \tag{5}$$

O_2 formed in acidic media can be reduced (Eq. (6)), where Eqs. (5) and (6) represent the so-called indirect HPRR mechanism.

$$O_2 + 4H^+ + 4e^- \rightarrow 2\,H_2O \quad E^0 = 1.23\ \text{V vs. SHE} \tag{6}$$

The direct reduction of H_2O_2, as a two-electron process, is dominant and certainly preferable to indirect process, due to its higher standard electrode potential [28]. Pt electrocatalysts have been extensively studied for direct HPPR [24], despite Pt being also active for H_2O_2 decomposition [29]. Pd [2,30,31], Ag [32], Au [33,34] and Cu [35] have been also studied for HPRR, as well as carbon-supported Pt and Pd electrocatalysts [4,36,37].

Considering the high performance of noble metal (e.g., Pt, Pd, Au) electrocatalysts, but also their high price, the scientific community has been devoted to finding alternative electrocatalysts of comparable performance, but lower price compared to the bulk counterparts. Different approaches have been studied, such as reducing the amount of metal used by decreasing its particle size. In addition, efficient dispersion methods to homogenize the distribution of those particles in the catalyst have been investigated [38]. Another popular and extensively used approach consists in the employment of a suitable support [38]. A good support must have high surface area, good conductivity, capacity to stabilize metal nanoparticles, resistance to corrosion in the reaction medium, as well as low price [39–41]. Choice of support and its properties are known to have an important effect on the electrocatalysts' performance [39].

Carbon-based support materials have been widely used due to their suitable properties, such as high surface area, good conductivity and porosity, as well as their accessible economic value, easy production and designable framework [39,42]. Among these carbon materials are carbon black [3,40,43], graphene and reduced graphene oxide [41,44] mesoporous carbons [44–47] and carbon nanotubes (CNTs) [48–50]. Graphene is a material known due to the strong interaction of its nanosheets with the metal nanoparticles, showing a great capacity of metal stabilization [51,52]. Mesoporous carbons are also becoming popular, since their surface and pore dimension can be easily modified and adapted [39,51]. CNTs, on the other hand, have been used due to their interesting chemical stability and high electronic conductivity [51]. Carbon blacks, such as commercially available Vulcan XC-72, Ketjen Black and Black Pearls, have been extensively used as supports due to their high conductivity and availability [34,42].

The good results obtained when combining small metallic particles and an adequate support have led to considerable improvements in the DBPFC performance. For example, Pd nanoparticles supported on two different biobased carbon materials (grape stalk activated carbon, GSAC, and vine shoots activated carbon, VSAC) were tested as electrocatalysts for BOR, with Pd/VSAC leading to a number of exchanged electrons of 5.6 [43]. Oh et al. studied different metals (Rh, Ru, Pt, Au, Ag, Pd, Ni and Cu) supported on multiwalled CNTs (MWCNTs) as electrocatalysts for DBPFC, reaching power density values as high as 135.5 mW cm^{-2} and 118.6 mW cm^{-2} by employing Pt/MWCNT (1 mg cm^{-2}) as anode and as cathode, respectively. In this work, the authors also observed that the MWCNT performance as support was higher than that obtained by using Vulcan XC72 in the same conditions [48]. Valiollahi and Ojani also analyzed the activity of Pt hollow nanospheres supported on graphene for BOR, reaching peak current density values above 50 mA cm^{-2} [53].

It is known that the electrode kinetics is strongly influenced by the surface characteristics of the carbon support and by the size of the metal nanoparticles [34,42]. Several studies towards the development of novel carbon-based support materials with improved surface properties for fuel cell applications have been done [51,54]. These studies suggest the use of carbon composite supports, including carbon-carbon, carbon-ceramic and carbon-polymer composites, which combine the advantages of the carbon material with important features of other compounds. Among the different types of composites, the carbon-polymer ones have attracted considerable attention since they demonstrate enhanced properties compared to their individual parent components [55]. In a carbon-polymer composite support, it is important that the polymer does not decrease the conductivity of the carbon material. Thus, conducting polymers such as polyaniline (PANI), polythiophene (PTh), poly (3,4-ethylenedioxythiophene) (PEDOT) and polypyrrole (PPy), are normally selected due to their good electronic and ionic conductivity, as well as high chemical stability [56–62]. Among them, PEDOT and PPy are the most widely used [57–62], with PPy being considered as the most attractive [56]. The combination of carbon black with conducting polymers, such as PEDOT or PPy, results in ideal composite supports with promising features for fuel cell applications [61,63,64]. Considering that, four PPy-C-supported Pt electrocatalysts containing different amounts of carbon black, were prepared and tested for BOR in alkaline media and for HPRR in acidic media using cyclic voltammetry (CV) and chronoamperometry (CA). Subsequently, laboratory DBPFCs with Pt/PPy-C as anode and/or cathode were assembled and tested, in order to assess the fuel cells' efficiency using these novel electrocatalyst materials.

2. Experimental

2.1. Synthesis and characterization of Pt/PPy-C materials

Synthesis of the PPy-C composites was carried out at room temperature by in situ chemical oxidative polymerization. Ammonium persulfate and p-toluene sulfonic acid were used as the oxidant and dopant, respectively, and the carbon (Vulcan XC-72, Cabot Corporation) amount in the PPy-C composites was varied between 5 and 35 wt.% to investigate the effect of the PPy amount on the supports' properties. The synthesis details can be found elsewhere [63]. Subsequently, Pt nanoparticles were anchored on the support materials by microwave irradiation technique. H_2PtCl_6 (0.05 M aqueous solution) was used as metal precursor and ethylene glycol was chosen as the reducing environment. Then, 0.1 g of the composite support and 2.6 mL of the aqueous solution of H_2PtCl_6 were added in 50 mL of ethylene glycol and stirred for a while. The resulting mixture was put into a domestic microwave oven and heated for 1 min at 800 W. The mixture was next cooled down with cold water, filtered, washed with acetone and deionized water and, finally, dried in a vacuum oven for 12 h [46]. As a result, PPy-C-supported Pt electrocatalysts were obtained.

Fourier-transform infrared (FTIR) spectra were collected on Bruker VERTEX 70v Infrared Spectrometer, while Raman spectra were collected using WITech Raman microscope alpha300 R with 532 nm excitation source at room temperature. X-ray photoelectron spectroscopy (XPS) analysis was carried out on Specs-Flex X-ray photoelectron spectrometer. Scanning electron microscopy with energy dispersive spectroscopy (SEM/EDS) analysis was done using Phenom ProX microscope. Inductively coupled plasma mass spectrometry (ICP-MS) analysis was performed using Agilent 7800 ICP mass spectrometer. Transmission electron microscopy (TEM) images were recorded using a JEOL 2100F (200 kV) high-resolution microscope.

2.2. BOR and HPRR studies

BOR and HPRR measurements were done using Gamry PCI4/750 Potentiostat/Galvanostat in a one-compartment electrochemical cell of 50 mL volume. A Pt electrode served as counter, while saturated calomel electrode (SCE) was employed as reference. All potentials within this paper are given relative to the reversible hydrogen electrode (RHE). Catalytic inks were prepared by ultrasonically dispersing 5 mg of the corresponding Pt/PPy-C electrocatalyst in 125 μL of 2% polyvinylidene difluoride solution in *N*-methyl 2-pyrrolidone for 30 min. Working electrodes were made by pipetting 10 μL of the corresponding catalytic ink onto a glassy carbon (GC) tip and leaving it to dry at 80 °C overnight.

BOR studies were done by cyclic voltammetry (CV) in 0.03 M $NaBH_4$ + 2 M NaOH solution from the open circuit potential (OCP) to 1.3 V using different scan rates (5–1000 mV s^{-1}) at 25 °C. Furthermore, CVs were recorded in a range of temperatures between 25 and 65 °C, controlling the temperature by water circulation using a Haaeke F3 bath. CVs were also recorded in solutions of different $NaBH_4$ concentrations (0.01–0.12 M) at 25 °C.

HPRR studies were done in 0.05 M H_2O_2 + 0.1 M HCl solution saturated with N_2. CV measurements were carried out scanning the potential from 1.0 to 0.1 V at different scan rates (5–1000 mV s^{-1}) at 25 °C. CV measurements were also run in a range of temperatures from 25 to 65 °C. It should be mentioned that HCl, H_2SO_4 and $HClO_4$ have been previously used as supporting electrolytes for HPRR fundamental studies, with the strength of the acid anions (Cl^-, SO_4^- and ClO_4^-) adsorption on the electrode surface being known to affect its activity for H_2O_2 reduction and the reaction pathways [37].

Finally, Pt/PPy-C electrode stability tests were carried out by recording chronoamperometric (CA) curves at −0.7 and 0.9 V for BOR and HPRR, respectively, during 1 h at 25 °C.

2.3. Fuel cell tests

A laboratory two-compartment acrylic DBPFC was assembled with catholyte and anolyte volume of 100 mL employing a Pt mesh (Johnson Matthey, A = 50 cm^2) and Pt/PPy-C (A = 4 cm^2 and A = 2.39 cm^2) as electrodes and Nafion 117 cation-exchange membrane (DuPont, Wilmington, DE) as separator. The distance between anode and cathode (3 cm) was set to be the lowest possible in order to minimize the ohmic losses. The distance between the electrodes and membrane was the same for both anode and cathode (1.5 cm). Nafion 117 was used as separator since thin membranes typically show low values of ohmic and transport resistance, which lead to an improvement of the fuel cell performance [65]. Additionally, Nafion 117 presents a conductivity of 83 mS cm^{-1}, notably higher compared to that of other commercial membranes, such as IONAC MC-3470 (40 mS cm^{-1}). Finally, Nafion 117 is one of the membranes with the highest transport resistance for BH_4^- ion, thus preventing the undesirable BH_4^- ion crossover and the generation of parasitic currents, which are responsible for decreasing the DBPFC performance [26].

For the cell tests, an adequate volume of catalytic ink was deposited onto polished GC electrodes (Table 1). 1 M $NaBH_4$ in 4 M NaOH solution was used as anolyte and 5 M H_2O_2 in 1.5 M HCl solution was used as catholyte – the composition of those electrolytes was chosen as previously reported to be optimal electrolytes compositions for DBPFCs [66]. DBPFC tests were done at room temperature on a PAR 273A (Princeton Applied Research, Inc.) potentiostat. During the tests, cell voltages (ΔE) between the open circuit voltage (OCV) and 0.15 V were applied and the corresponding cell currents after stabilization were recorded. The geometric area of the Pt/PPy-C electrode (cathode or anode, A = 4 cm^2) was used for calculation of all cell current densities, except for the case of the DBPFC using Pt/PPy-C both as cathode and as anode, where the smaller area of the anode (A = 2.39 cm^2) was used.

Table 1
General description of the electrodes used during DBPFC laboratory tests, including the electrodes area and electrocatalysts loading.

Experiment	Anode	Cathode
Pt/PPy-C anode & cathode	Pt/PPy-C, A = 2.39 cm^2 (0.33 mg cm^{-2})	Pt/PPy-C, A = 4 cm^2 (1.0 mg cm^{-2})
Pt/PPy-C anode	Pt/PPy-C, A = 4 cm^2 (0.40 mg cm^{-2})	Pt mesh, A = 50 cm^2
Pt/PPy-C cathode	Pt mesh, A = 50 cm^2	Pt/PPy-C, A = 4 cm^2 (0.40 mg cm^{-2})

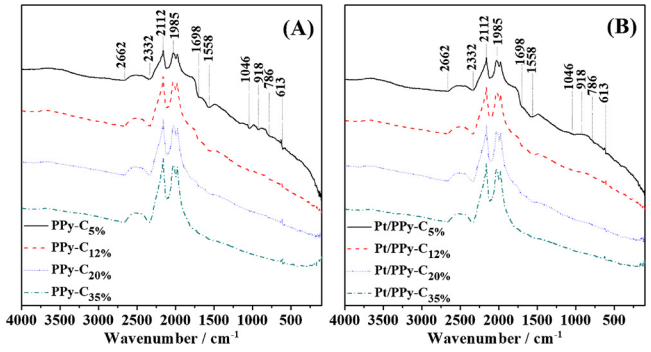

Fig. 1. FTIR spectra of (A) PPy-C composites and (B) Pt/PPy-C electrocatalysts.

3. Results and discussion

3.1. Characterization of Pt/PPy-C electrocatalyst

FTIR spectra of the prepared composites (PPy-C) and catalysts (Pt/PPy-C) are shown in Fig. 1. The main vibration peaks of PPy at 786 and 918 cm^{-1} are due to the presence of polymerized pyrrole, while the peak at 613 cm^{-1} corresponds to N—H out-of-plane vibration [63,67]. The peak at 1046 cm^{-1} is due to the C—H and N—H in-plane-deformation vibration of the pyrrole ring [68]. The peaks at 1558 and 1698 cm^{-1} are attributed to the carbonyl group and to the C=C/C—C ring stretching of pyrrole. The sharp peak at 2112 cm^{-1} is assigned to the C≡C stretch vibration and the peak at 2332 cm^{-1} is attributed to the presence of the C=S group. Thus, FTIR spectroscopy results indicate possible interaction between PPy and carbon particles. The intensity of the characteristic peaks are found to vary in the composites containing 5–35 wt.% carbon. The clearest vibration modes are observed in PPy-$C_{5\%}$ composite. Additionally, no shift of the bands was observed upon grafting Pt nanoparticles onto PPy-C.

Raman spectroscopy is a technique widely used to characterize carbon-based materials and composites [69,70]. In the case of the carbon-polymer composites, Raman spectroscopy is used to analyze the interactions between the carbon material and the polymer chains, since those determine the final properties of the material. According to the literature, this interaction is demonstrated by a shift of the peaks, by a peak width change and also by the differences in the ratio of D and G bands intensity [69,71,72]. Thus, the PPy-C and Pt/PPy-C samples were analyzed by Raman spectroscopy, as shown in Fig. 2. The vibrational band appearing at ca. 1346 cm^{-1}, known as D or Defect band, is assigned to the ring-stretching mode of PPy and edges of the graphite crystallites [72,73]. The G band at ca. 1581 cm^{-1} is ascribed to ordered graphite crystallites and to the C=C backbone stretching of PPy [74–76]. The ratio of the D and G band intensities (I_D/I_G) often indicates the disordered nature of the prepared structures, and it was observed to be 0.97, 0.83, 0.62, 0.84 for PPy-$C_{35\%}$, PPy-$C_{20\%}$, PPy-$C_{12\%}$, PPy-$C_{5\%}$ support materials, respectively. It was seen that the number of defects in the composites' structure increased with the addition of carbon to PPy.

In order to see whether microwave treatment affects the number of

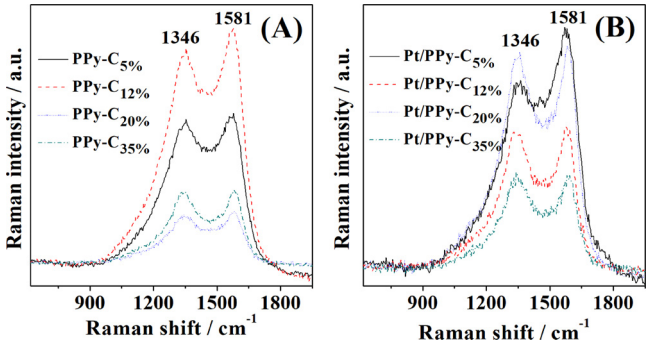

Fig. 2. Raman spectra of (A) PPy-C composites and (B) Pt/PPy-C electrocatalysts.

defect sites, Raman analysis of PPy-C composite materials treated by microwave heating was carried out (Fig. S1 of electronic supplementary information, ESI). I_D/I_G ratios decreased after microwave heating, showing that the number of defect sites also decreased (Table S1 of ESI). Additionally, decoration of Pt nanoparticles over support materials resulted in an increase in I_D/I_G ratios to 1.06, 0.94, 0.87, 0.35 for Pt/PPy-$C_{35\%}$, Pt/PPy-$C_{20\%}$, Pt/PPy-$C_{12\%}$, Pt/PPy-$C_{5\%}$, respectively, which can be attributed to further defects formation in the electrocatalyst with the addition of Pt to the structure. Both PPy-$C_{35\%}$ support material and Pt/PPy-$C_{35\%}$ catalyst showed the highest I_D/I_G ratio revealing the highest number of defects when compared to other materials. The intensity in the Raman spectra also decreased for the materials having higher carbon content due to the amorphization of the material [77], which is related with the formation of more defects with the addition of carbon black [78].

XPS was used to elucidate the chemistry of the synthesized electrocatalysts (Figs. 3 and S2). It revealed the presence of C1s, O1s, Pt4f, Pt4d, and N1s in all electrocatalysts. The oxygen element comes from oxidized form of PPy or oxygen containing groups on carbon surface [57]. The nitrogen element comes from the PPy backbone, and the presence of N in the structure is believed to be responsible for the improved activity towards various electrochemical reactions [79]. The details of the atomic composition of the electrocatalysts are listed in Table 2. A pronounced C1s signal appears at 284 eV and a minor signal at 286.3 eV, which refers to different bonding of C with N or O, as observed in all electrocatalysts. As expected, sp^2 C increases with the C amount in the electrocatalysts (Table 2). In the spectrum (Fig. S2), $Pt4f_{7/2}$ and $Pt4f_{5/2}$, with 71.2 and 74.6 eV binding energies, respectively, display the strongest signals, showing that metallic Pt is predominant in the electrocatalysts. The Pt4d doublet appears at ca. 331.4 and 314.5 eV binding energies [57,80].

The TEM images of the four electrocatalysts given in Fig. 4 show the homogeneity of the Pt nanoparticles over the composite support

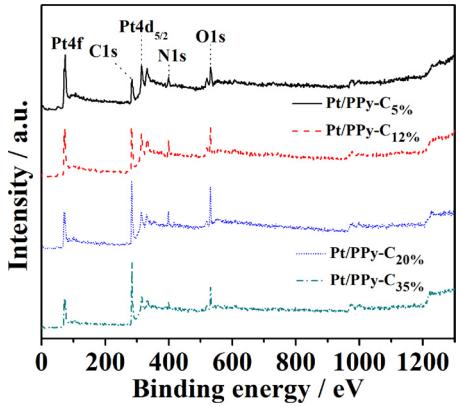

Fig. 3. XPS spectra of Pt/PPy-C electrocatalysts.

Table 2
Surface composition of the electrocatalysts as determined by XPS analysis.

Catalysts	Composition/wt.%				
	O1s	C1s	N1s	Pt4d	Pt4f
Pt/PPy-$C_{5\%}$	15.7	47.9	12.5	10.9	13
Pt/PPy-$C_{12\%}$	20.1	53	13.2	6.8	6.9
Pt/PPy-$C_{20\%}$	15.9	61.9	12.7	5.5	4
Pt/PPy-$C_{35\%}$	13	67.7	10.4	4.6	4.3

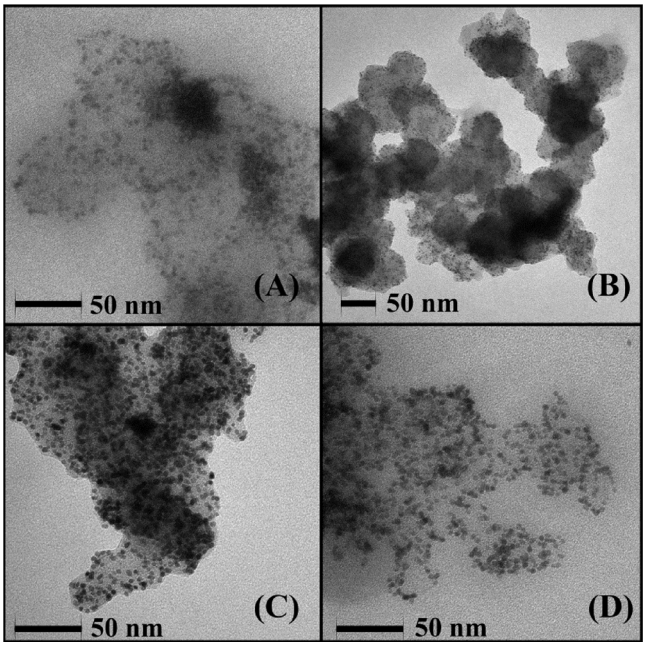

Fig. 4. TEM images of (A) Pt/PPy-$C_{5\%}$, (B) Pt/PPy-$C_{12\%}$, (C) Pt/PPy-$C_{20\%}$, and (D) Pt/PPy-$C_{35\%}$ electrocatalysts.

materials. The analysis revealed that well dispersed, spherical Pt nanoparticles were obtained on the surface of PPy-C composite supports, with particle sizes ranging between 3–4 nm.

Fig. 5 illustrates the morphology of the electrocatalyst materials observed by SEM, with the corresponding EDS data shown as inset confirming the presence of C, O, N and Pt. Table 3 shows that the Pt loading on the PPy-C composites, as determined by ICP-MS, ranged between 10.5 and 14.6 wt.%.

3.2. Oxidation of BH_4^- at Pt/PPy-C electrocatalysts

$NaBH_4$ oxidation at Pt/PPy-C electrocatalysts was observed by CV in 0.03 M $NaBH_4$ + 2 M NaOH solution in potential range from OCP to 1.3 V at scan rate of 50 mV s^{-1} and temperature of 25 °C. CVs of the four Pt/PPy-C electrocatalysts, shown in Fig. 6A, reveal similarities in the characteristic peaks (peak a_1, in the 0.3–0.6 V potential range, peak a_2 in the 0.6–1.0 V range, and peak a_3 in the 0.74–1.08 V range). Namely, these CVs acquired under natural diffusion conditions illustrate the BOR complexity indicating that CV response is governed by both BH_4^- hydrolysis (i.e., oxidation of its products) and BH_4^- direct oxidation at the studied electrocatalysts. Assignment of these peaks has been previously discussed in the literature, but there are still some uncertainties [2,3,81,82]. CVs of Pt/PPy-$C_{5\%}$, Pt/PPy-$C_{12\%}$ and Pt/PPy-$C_{20\%}$ reveal additional oxidation peak c_1 on the cathodic scan corresponding to the oxidation of BH_3OH^- adsorbed during the anodic scan [3,81,82]. Peaks a_1 and c_1 did not appear at CV of Pt/PPy-$C_{35\%}$, suggesting this electrocatalyst as the least active for BH_4^- hydrolysis (no formation and subsequent oxidation of its hydrolysis products) and the

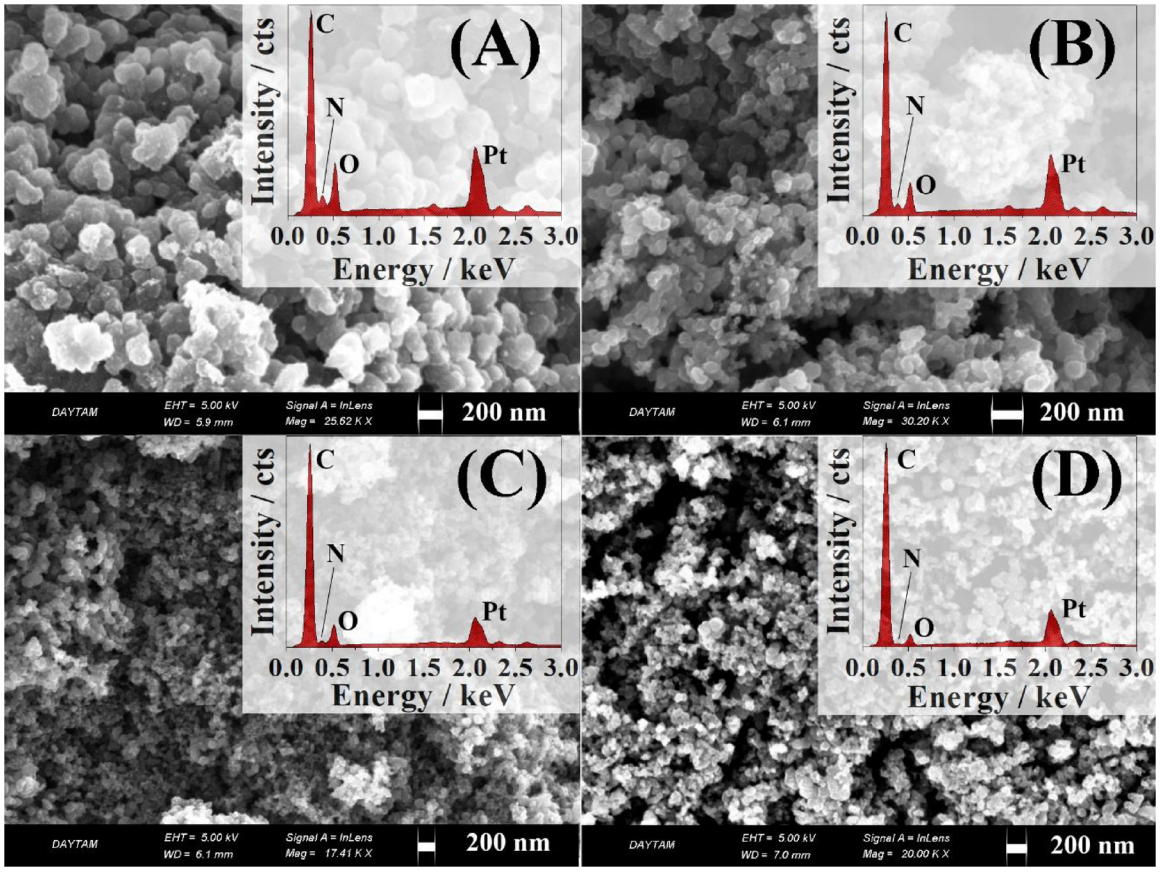

Fig. 5. SEM images with corresponding EDS data of (A) Pt/PPy-$C_{5\%}$, (B) Pt/PPy-$C_{12\%}$, (C) Pt/PPy-$C_{20\%}$, and (D) Pt/PPy-$C_{35\%}$ electrocatalysts.

Table 3
Pt loading (wt.%) in the electrocatalysts as determined by ICP-MS.

Catalysts	Pt loading/wt.%
Pt/PPy-$C_{5\%}$	14.2
Pt/PPy-$C_{12\%}$	11.0
Pt/PPy-$C_{20\%}$	10.5
Pt/PPy-$C_{35\%}$	14.6

most active for BH_4^- direct oxidation. Hence, Pt/PPy-$C_{35\%}$ gave the best response during BOR, i.e., the highest current density of ca. 28 mA cm^{-2}, while Pt/PPy-$C_{5\%}$ gave the lowest current density of ca. 7 mA cm^{-2} at 0.74 V. OCP was found to be ca. 0.1 V for Pt/PPy-$C_{20\%}$ and Pt/PPy-$C_{35\%}$, and 0.0 V for Pt/PPy-$C_{5\%}$ and Pt/PPy-$C_{12\%}$. These values are somewhat lower than the theoretical value of the standard potential of BH_4^- oxidation (−1.24 V vs. SHE) due to the mixed potentials, as BH_4^- hydrolysis (Eq. (2)) and oxidation of its products proceed in parallel with BOR. Namely, the cathodic hydrogen evolution reaction (HER) at Pt electrodes was reported to be faster than the BOR in the lower potential region, resulting in the BOR OCP close to the hydrogen reversible potential [22,83]. Thus, OCP values result from the competition between BOR and HER.

Furthermore, performance of Pt/PPy-C catalysts for BOR was compared to that of commercial Pt/C catalysts. Fig. 6B illustrates CVs of Pt/PPy-$C_{35\%}$ and Pt/C recorded in 0.03 M $NaBH_4$ + 2 M NaOH solution under the same conditions. Pt/PPy-$C_{35\%}$ gives somewhat higher BOR current densities compared to Pt/C. However, this difference becomes clearer once specific current densities (current density per mg of Pt) are compared. Namely, a j_p value of 446 mA mg_{Pt}^{-1} (28 mA cm^{-2}) was achieved at 0.70 V for Pt/PPy-$C_{35\%}$, a value ca. 30 times higher than that obtained using a Pt/C catalyst (15 mA mg_{Pt}^{-1} or 22 mA cm^{-2} at

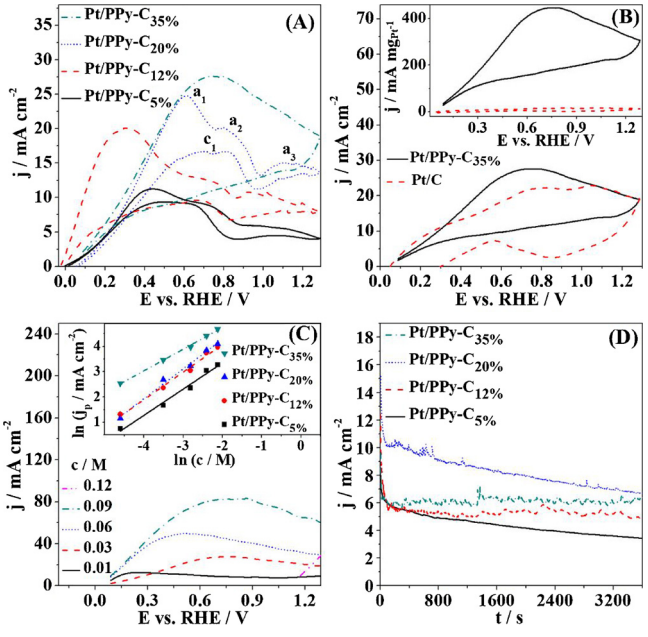

Fig. 6. (A) CVs of the four Pt/PPy-C electrocatalysts at 50 mV s^{-1}. (B) CVs of Pt/PPy-$C_{5\%}$ and commercial Pt/C presenting the current density and mass-specific current density (inset) values at 50 mV s^{-1}. (C) Anodic scans of Pt/PPy-$C_{35\%}$ in $NaBH_4$ solutions of different concentrations (0.01–0.12 M) at 50 mV s^{-1} with corresponding ln j_p vs. ln c plots for all electrocatalysts in inset. (D) CA stability test for the four Pt/PPy-C electrocatalysts at 0.4 V during 1 h. Measurements done in 0.03 M $NaBH_4$ + 2 M NaOH and temperature of 25 °C unless otherwise specified.

Table 4
Kinetic parameters of BOR at Pt/PPy-C electrocatalysts.

Electrocatalyst	n	E_a/kJ mol^{-1}	α	β
Pt/PPy-$C_{5\%}$	6.5	18	0.42	1.03
Pt/PPy-$C_{12\%}$	6.0	13	0.75	1.09
Pt/PPy-$C_{20\%}$	7.2	15	0.83	1.17
Pt/PPy-$C_{35\%}$	7.6	10	0.94	0.85

0.8 V). Although one of the obvious advantages of PPy is the catalyst enhanced stability, it has also been reported that nanostructured and mixed-conducting PPy as a component of Pt catalyst supports enables setting up an effective conducting network for charge transfer and may improve the surface morphology for the Pt deposition. In fact, carbon particles and PPy seem to be not just mechanically mixed, but actually well incorporated in each other. Such a good dispersion acts as a good charge transfer channel and reduces the electric resistance at the interface.

BOR at the four Pt/PPy-C electrocatalysts was next investigated by CV in 0.03 M $NaBH_4$ + 2 M NaOH solution at different scan rate in range from 5 to 1000 mV s^{-1} at temperature of 25 °C (Fig. S3A). It was observed that increasing the scan rate, peak a_3 shifts to more positive potential values (this shift becomes noticeable at higher scan rates) along with increase of peak current density. Anodic charge transfer coefficient, α, values for BOR at Pt/PPy-$C_{5\%}$, Pt/PPy-$C_{12\%}$, Pt/PPy-$C_{20\%}$ and Pt/PPy-$C_{35\%}$, evaluated from the E_p vs. ln $\nu^{1/2}$ plot [84], were found to be 0.42, 0.75, 0.83 and 0.94, respectively (Table 4 and Fig. S3B). Number of exchanged electrons, n, during BOR at four Pt/PPy-C electrocatalysts, calculated from the slope of j_p vs. $\nu^{1/2}$ plots [84] (Fig. S3C), was found to range from 6.0 to 7.6 (Table 4). These values are higher or comparable with typical n values reported in the literature for BOR at Pt or Pt alloys (2–6 electrons) [1,3,82,85–88].

CVs recorded in $NaBH_4$ solutions of different concentrations revealed that the increase of $NaBH_4$ concentration leads to an increase of peak current densities [89], e.g., Pt/PPy-$C_{35\%}$ gave peak current density of 12 mA cm^{-2} in 0.01 M $NaBH_4$ + 2 M NaOH solution and ca. ten times higher value of 107 mA cm^{-2} in 0.12 M $NaBH_4$ + 2 M NaOH solution. The reaction order of BOR at the four Pt/PPy-C electrocatalysts was evaluated from the CV data for different $NaBH_4$ concentrations (0.01–0.12 M) (Fig. 6C) using Eq. (7) [89],

$$j_p = zc^{\beta} \quad (7)$$

where j_p is the peak current density (mA cm^{-2}), z is a constant, c is $NaBH_4$ concentration and β is the order of the reaction with respect to BH_4^-. The value of β was determined from the slope of ln j_p vs. ln c plot and found to be in the 0.85–1.17 range for all tested electrocatalysts (Table 4). These values are in agreement with those reported in the literature, which are typically close to 1 [1–3,13].

BOR at Pt electrodes was reported to occur via different mechanisms depending on $NaBH_4$ concentration [6]. Thus, it was reported that at low concentrations, BOR proceeds by "partially-dissociative" BH_{3ads} mechanism (with formation of H_2) below the OCP region and in the Pt-oxide region at potential values higher than ca. 0.7 V and by the "fully-dissociative" BH_{ads} mechanism between the OCP and 0.7 V. On the other hand, at sufficiently high concentrations of $NaBH_4$, BOR mainly proceeds via "partially-dissociative" BH_{3ads} mechanism regardless the potential values so that H_2 is generated in the whole potential region. The latter might be due to the poisoning of Pt electrode surface by adsorption of BOR intermediates. Therefore, stability of the four Pt/PPy-C electrocatalysts activity for BH_4^- oxidation was investigated by chronoamperometric (CA) studies. Previous studies of Pt poisoning during BOR found it to be a complex process dependent on the electrode potential [90]. Thus, poisoning by adsorption of reaction intermediates occurs rapidly when Pt surface hydrides are present, i.e., in the low potential region (0.14–0.84 V), being most pronounced in the

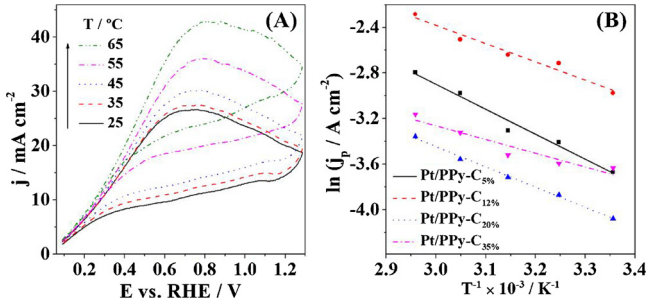

Fig. 7. (A) CVs of Pt/PPy-$C_{35\%}$ in 0.03 M $NaBH_4$ + 2 M NaOH at 50 mV s^{-1} in the 25–65 °C temperature range and (B) corresponding Arrhenius' regressions (ln j_p vs. T^{-1}) of the four electrocatalysts.

0.14–0.34 V region. Moving to more positive potential of 0.9 V, where neither surface hydrides nor surface oxides are present, a self-cleaning process, i.e. oxidation of adsorbed intermediates, proceeds. Further increasing the potential to 1.34 V, where some Pt surface oxides are present, poisoning again occurs rapidly. At potentials above 1.44 V, where the formed Pt oxides cover the whole electrode surface, oxidation of adsorbed intermediates again occurs, thus cleaning the electrode surface and enabling re-establishment of BOR currents that were observed at lower potentials [90]. Fig. 6D shows CA stability tests done in 0.03 M $NaBH_4$ + 2 M NaOH solution at 0.4 V during 1 h. A gradual decrease of the current density could be observed for Pt/PPy-$C_{5\%}$ and Pt/PPy-$C_{20\%}$, while current density was observed to be stable at Pt/PPy-$C_{12\%}$ and Pt/PPy-$C_{35\%}$.

CVs data of the four Pt/PPy-C electrocatalysts in 0.03 M $NaBH_4$ + 2 M NaOH at different temperatures (25–65 °C) (Fig. 7A) were used for determination of the apparent activation energy, E_a^{app}, from Arrhenius equation (Eq. (8)), assuming that E_a^{app} does not depend on the temperature [3,91].

$$\frac{\partial \ln|j|}{\partial(1/T)} = \frac{\Delta E_a^{app}}{R} \quad (8)$$

Arrhenius' regressions (ln j_p vs. T^{-1}) were constructed for each electrocatalyst (Fig. 7B), and their slopes were used for determination of the E_a^{app} values. Pt/PPy-$C_{35\%}$ showed the lowest E_a^{app} (10 kJ mol^{-1}), while Pt/PPy-$C_{5\%}$ gave the highest value of ca. 18 kJ mol^{-1} (Table 4). These values are lower than those reported for BOR at other Pt-based electrocatalysts; for instance, E_a^{app} for BOR at PtDy alloys was reported to be 29 kJ mol^{-1} [1] and at carbon-supported Pt bimetallic (PtM/C, M = Ni, Co) alloys it ranged between 20 and 34 kJ mol^{-1} [3].

3.3. Reduction of H_2O_2 at Pt/PPy-C electrocatalysts

CVs of four Pt/PPy-C electrocatalysts in N_2-saturated 0.05 M H_2O_2 + 0.1 M HCl solution recorded scanning the potential from 1.0 to 0.3 V at 50 mV s^{-1} and at 25 °C are shown in Fig. 8A. It is evident that Pt/PPy-$C_{35\%}$ electrocatalyst gives the best electrochemical response during HPRR, i.e., it gives a noticeable cathodic peak of the highest (i.e., the most negative) current density among the four Pt/PPy-C electrocatalysts. Namely, current densities for Pt/PPy-$C_{5\%}$, Pt/PPy-$C_{12\%}$, Pt/PPy-$C_{20\%}$ and Pt/PPy-$C_{35\%}$ at ca. 0.8 V amounted to −0.52, −1.24, −2.1 and −2.9 mA cm^{-2}, respectively.

Further studies were done by running CVs at different scan rates ranging from 10 to 1000 mV s^{-1} (Fig. S4A) and at different temperatures (Fig. 8B). A shift of peak potential to more negative values and increase of the reduction peak (i.e., more negative current densities) with the increase of scan rate was observed for all Pt/PPy-C electrocatalysts (Fig. S4B,C illustrates the case of Pt/PPy-$C_{35\%}$). From this set of data, cathodic charge transfer coefficient, α, values in the 0.66–0.83 range were obtained for HPRR at the four Pt/PPy-C electrocatalysts, as shown in Table 5. Number of electrons exchanged, n, during HPRR

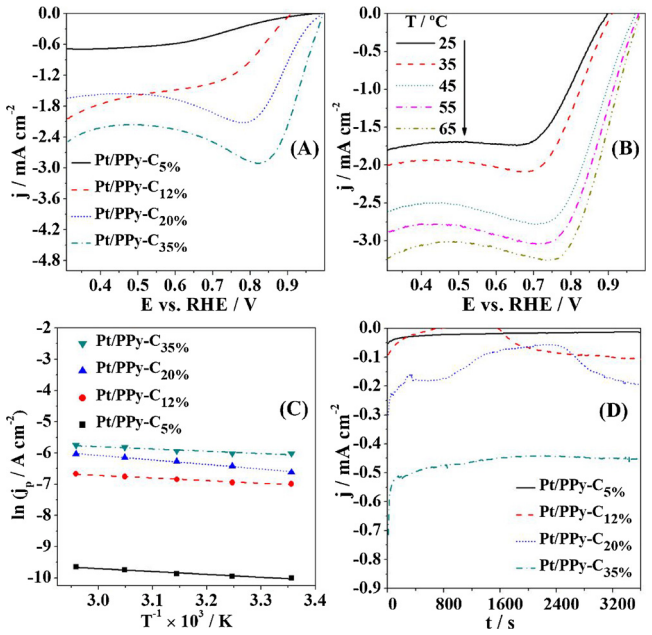

Fig. 8. Cathodic scans of (A) the four Pt/PPy-C electrocatalysts and of (B) Pt/PPy-$C_{35\%}$ at temperatures ranging from 25 to 65 °C. (C) Arrhenius plots and (D) chronoamperometric stability tests for the Pt/PPyC electrocatalysts at 0.9 V during 1 h. All measurements done in N_2-saturated 0.05 M H_2O_2 + 0.1 M HCl at 50 mV s^{-1} and 25 °C, unless otherwise noted.

Table 5
Kinetic parameters for HPRR at Pt/PPy-C electrocatalysts.

Electrocatalyst	n	E_a/kJ mol^{-1}	α
Pt/PPy-$C_{5\%}$	–	14	0.83
Pt/PPy-$C_{12\%}$	1.0	8	0.66
Pt/PPy-$C_{20\%}$	1.0	11	0.75
Pt/PPy-$C_{35\%}$	2.0	8	0.77

value was found to be 1.0 for Pt/PPy-$C_{12\%}$ and Pt/PPy-$C_{20\%}$. A higher n value of 2.0 was obtained at Pt/PPy-$C_{35\%}$, indicating an increase of the electrocatalytic activity for HPRR with increase of the carbon amount in Pt/PPy-C electrocatalysts.

CV data collected at different temperatures were used for calculation of E_a^{app} using Eq. (8) (Fig. 8C). Thus, E_a^{app} values were calculated from the slope of the Arrhenius plots and found to be 14 kJ mol^{-1} for Pt/PPy-$C_{5\%}$, 11 kJ mol^{-1} for Pt/PPy-$C_{20\%}$, and ca. 8 kJ mol^{-1} for Pt/PPy-$C_{12\%}$ and Pt/PPy-$C_{35\%}$. HPRR proceeds with low E_a^{app} at Pt/PPy-$C_{35\%}$, in agreement with high activity that this electrocatalyst showed for HPRR. E_a^{app} values obtained by Cardoso et al. for HPRR at Pt, Pt-Ho and Pt-Sm alloys fit in the 14–20 kJ mol^{-1} range [24]. However, Santos et al. found that E_a^{app} values for HPRR at Ni-RE (RE = Ce, Sm and Dy) alloys ranged between 38 and 46 kJ mol^{-1}, being significantly higher than E_a^{app} values obtained herein [92].

A chronoamperometric study was performed for the four Pt/PPy-C electrocatalysts in order to analyze their stability in N_2-saturated 0.05 M H_2O_2 + 0.1 M HCl solution at 0.9 V and 25 °C, during 1 h (Fig. 8D). This study revealed changes in the HPRR activity of Pt/PPy-$C_{12\%}$ and Pt/PPy-$C_{20\%}$ (i.e., change of current density) with time. On the other hand, Pt/PPy-$C_{5\%}$ and Pt/PPy-$C_{35\%}$ exhibited a stable activity (i.e., constant current density) during the experiment. However, current density at Pt/PPy-$C_{5\%}$ stabilized at value close to zero confirming negligible activity of this electrocatalyst for HPRR. Contrary, Pt/PPy-$C_{35\%}$ achieved the most negative current density value (at the end of the stability test) among all catalysts, in agreement with the CV studies.

Previous studies using Pt/C electrocatalyst for HPRR, in similar conditions to those used in the present work (0.03 M H_2O_2 + 0.1 M $HClO_4$ at room temperature), reported a specific current density of −5.1 mA mg_{Pt}^{-1} (−0.4 mA cm^{-2}) at 0.85 V and 10 mV s^{-1} [37], a value 3.2 times lower than the obtained for Pt/PPy-$C_{35\%}$ (−16.4 mA mg_{Pt}^{-1} or −1.0 mA cm^{-2}) in 0.05 M H_2O_2 + 0.1 M HCl solution. This shows that Pt/PPy-C materials are also promising cathodic catalysts for DBPFCs.

3.4. Fuel cell tests

To evaluate the performance of Pt/PPy-C as cathode or as anode for a DBPFC, cell tests using a Pt mesh as anode/cathode and a Pt/PPy-C cathode/anode were performed. The polarization and power densities curves were recorded for each electrocatalyst tested, as shown in Fig. 9A,B. The employment of a Pt mesh in the opposite side of the evaluated electrode is justified by higher area and higher activity of Pt electrode for BOR and for HPRR [24,36,37]. Thus, it is possible to conclude that DBPFC performance, during the evaluation of Pt/PPy-C as cathode or as anode, was limited by Pt/PPy-C activity for HPRR or BOR, respectively.

Table 6 summarizes the obtained results for each electrocatalyst, where P_{max} (mW cm^{-2} or W g_{Pt}^{-1}) is the peak power density, and j_{max} (mA cm^{-2} or A g_{Pt}^{-1}) and ΔE_{max} (V) are the current density and cell voltage at P_{max}, All DBPFCs using a Pt/PPy-C cathode or anode presented a similar open circuit voltage (OCV) of ca. 1.8 V. This value is lower than the theoretical OCV value for a DBPFC using an acidic catholyte [65], due to the mixed overpotentials [1]. However, it is worth noting that the obtained OCV values are similar to those reported in literature for DBPFCs operating under similar conditions [93–97].

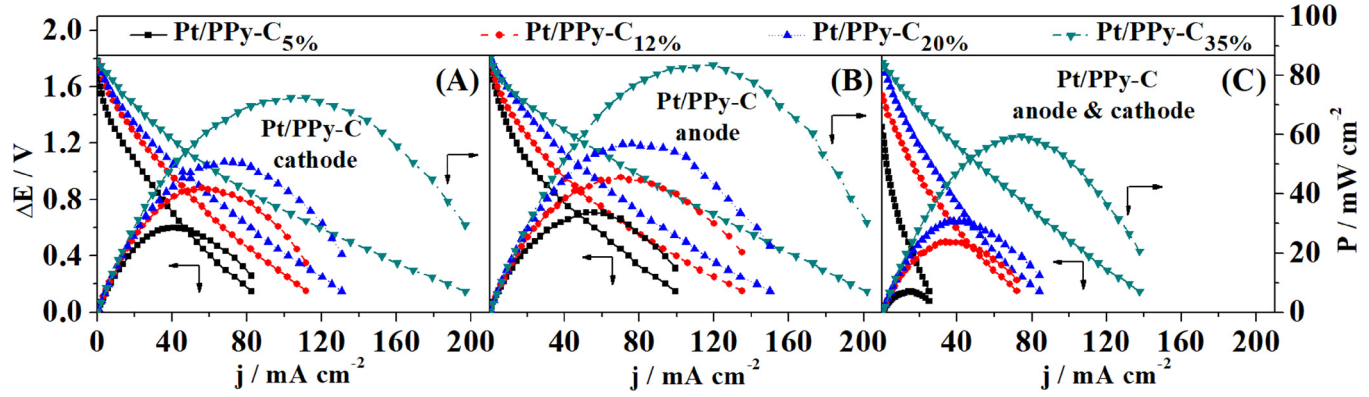

Fig. 9. Polarization (ΔE vs. j) and power density (P vs. j) curves at room temperature for DBPFC laboratory test using: (A) Pt/PPy-$C_{x\%}$ (x = 5, 12, 20 or 35) cathode and Pt mesh anode; (B) Pt/PPy-$C_{x\%}$ anode and Pt mesh cathode; (C) Pt/PPy-$C_{x\%}$ as both anode (A = 2.39 cm^2) and cathode (A = 4 cm^2). 1 M $NaBH_4$ + 4 M NaOH fuel, 5 M H_2O_2 + 1.5 HCl oxidant and a Nafion 117 membrane separator were used in all experiments.

Table 6
Summary of DBPFC performance parameters with Pt/PPy-C anode and/or cathode.

	Platinum loading/$mg_{Pt}\,cm^{-2}$	Electrode	P_{max}/mW cm^{-2}	P^{*}_{max}/W g_{Pt}^{-1}	j_{max}/mA cm^{-2}	j^{*}_{max}/A g_{Pt}^{-1}	ΔE_{max}/V	OCV/V
Pt/PPy-C cathode	0.06	Pt/PPy-$C_{5\%}$	28.7	505	14.0	722	0.70	1.79
	0.04	Pt/PPy-$C_{12\%}$	42.0	954	56.0	1273	0.75	1.78
	0.04	Pt/PPy-$C_{20\%}$	50.8	1210	67.8	1613	0.75	1.77
	0.06	Pt/PPy-$C_{35\%}$	72.5	1241	111.5	1909	0.65	1.78
Pt/PPy-C anode	0.06	Pt/PPy-$C_{5\%}$	33.6	592	51.8	911	0.65	1.81
	0.04	Pt/PPy-$C_{12\%}$	45.7	1038	70.3	1597	0.65	1.81
	0.04	Pt/PPy-$C_{20\%}$	57.0	1357	76.0	1810	0.75	1.81
	0.06	Pt/PPy-$C_{35\%}$	83.7	1432	119.5	2046	0.70	1.81
Pt/PPy-C anode & cathode	0.05[a], 0.14[c]	Pt/PPy-$C_{5\%}$	7.0	147	14.0	294	0.50	1.31
	0.04[a], 0.11[c]	Pt/PPy-$C_{12\%}$	23.7	644	33.9	920	0.70	1.54
	0.04[a], 0.11[c]	Pt/PPy-$C_{20\%}$	30.7	873	38.4	1092	0.80	1.75
	0.05[a], 0.15[c]	Pt/PPy-$C_{35\%}$	59.6	1219	74.5	1524	0.80	1.77

[a]Loading at anode, [c]loading at cathode; P^{*}_{max} and j^{*}_{max} stand for the mass-specific peak power density and corresponding mass-specific peak current density.

It could be observed that for the DBPFCs with Pt/PPy-C as cathode or as anode (Fig. 9A,B), the power density increases with the increase of the carbon amount in the electrocatalyst. This behavior could be explained by a better dispersion of Pt nanoparticles on the support for electrocatalysts with higher carbon amount, which leads to higher surface area of the electrocatalyst, as previously reported for a PEM fuel cell using Pt/PPy-C [61]. Furthermore, the addition of carbon can lead to higher conductivity – although PPy is a polymer with good electronic conductivity [98], carbon black has higher electronic conductivity [4].

Performance of Pt-based electrocatalysts observed in fundamental studies was found to not be fully maintained in practical fuel cell conditions. Namely, recent studies on the performance of Pt (as well as on Au and Pd) by Chatenet et al. [22] in $NaBH_4$ solutions of high concentration, corresponding to DBPFC operating conditions, reveal worsening of its performance with $NaBH_4$ concentration increase. Though BOR on Pt proceeds at higher rate compared to, for instance Au and Pd, the charge transfer kinetics becomes sluggish at high $NaBH_4$ concentration. The poisoning of Pt surface by BH_{ads} or $BH_{3,ads}$ intermediates becomes notable, further resulting in notable shift of the anode OCP, as well as significant reduction of the maximal recorded current. High $NaBH_4$ concentrations cause significant generation of H_2 gas, by either heterogeneous BH_4^- hydrolysis, dehydrogenation of BOR adsorbates, non-valorization of H_{ads} or from local pH variation at the electrode electrolyte interface. Still, as discussed below, data presented in Table 7 reveal that our fuel cell performance (in terms of power density) is comparable or higher than that of DBPFCs employing different carbon-supported Pt-based electrocatalysts and polymer-based electrocatalysts reported in the literature.

Next, the employment of Pt/PPy-C simultaneously as both anode and cathode of the laboratory DBPFC was tested. As shown in Table 1, an electrode with higher surface area and higher loading of the electrocatalyst was used on the cathode side because of to the previously mentioned cathode-limited cell performance. Polarization and power density curves are represented in Fig. 9C and Pt/PPy-C DBPFC performance parameters are also included in Table 6. Fig. S5 of Supplementary information shows the corresponding mass-specific (i.e., per gram of Pt loading in Pt/PPy-C catalysts) polarization and power density curves.

OCVs obtained for Pt/PPy-C DBPFCs are in the 1.31–1.77 V range. Similar OCV values were registered for electrocatalysts with 20% and 35% of carbon in the support, i.e., 1.75 and 1.77 V, respectively. Maximum power density of Pt/PPy-C DBPFCs increased when increasing the carbon content.

For a better assessment of the performance of Pt/PPy-C-based DBPFCs, Table 7 shows data on similar previously reported DBPFC catalysts. For instance, Oh et al. [48] obtained a P_{max} of 136 W g_{Pt}^{-1} using a Pt supported on multiwalled carbon nanotubes (Pt/MWCNTs) as anode and an Au cathode, a value 4.4 times lower than the value obtained using a Pt/PPy-$C_{5\%}$ as anode (592 W g_{Pt}^{-1}). The same authors obtained a value of 118 W g_{Pt}^{-1} in the cathode test employing Pt/MWCNTs as cathode and Pd as anode, i.e., 4.3 times lower value than the value obtained within cathode test using Pt/PPy-$C_{5\%}$ (505 W g_{Pt}^{-1}). Bayatsarmadi et al. [10] performed a study using different Pt electrocatalysts deposited on PPy as anode and cathode, obtaining P_{max} values in the range 30–112 W g_{Pt}^{-1}. It should be noted that different oxidant and fuel concentrations were used in the two studies. Regarding the Pt/C DBPFCs performance reported in literature, maximum power density of 47.6 W g_{Pt}^{-1} was reported by Yi et al. [93], using similar oxidant and fuel compositions (Table 7). This value is 12.5 times lower than that obtained for Pt/PPy-$C_{5\%}$ (592 W g_{Pt}^{-1}) and 30 times lower than that obtained for Pt/PPy-$C_{35\%}$ (1432 W g_{Pt}^{-1}). These comparisons show that PPy-carbon composites are promising supports for DBPFC electrocatalysts.

4. Conclusions

In this work, four Pt/PPy-C electrocatalysts were prepared and characterized using FTIR, Raman, XPS, SEM/EDS and ICP-MS. They were subsequently tested for BH_4^- oxidation in alkaline media and for H_2O_2 reduction in acidic media by CV and CA methods.

CVs of Pt/PPy-$C_{35\%}$ indicated its highest activity for BOR with an almost complete oxidation of BH_4^- and negligible activity for the undesirable BH_4^- hydrolysis concurrent reaction (absence of peak a_1). Considering kinetic parameters determined for BOR at Pt/PPy-C electrocatalysts, it was verified that Pt/PPy-$C_{35\%}$ presented the best features for BOR, with n of 7.6 and the lowest E_a of 10 kJ mol^{-1}. In addition, Pt/PPy-$C_{35\%}$ exhibited high stability during BOR chronoamperometric studies performed.

Regarding the performance of Pt/PPy-C electrocatalysts for HPRR, high activity of Pt/PPy-$C_{35\%}$ for HPRR could also be observed during CV studies, presenting a well-defined peak. Its best catalytic performance for HPRR was supported by an n of 2.0 and the lowest E_a value of 8 kJ mol^{-1}.

The fuel cell studies revealed an increased efficiency of DBPFC with the increase of carbon content in Pt/PPy-C catalysts, a result in agreement with those obtained for BOR and HPRR during the half-cell studies. Thus, Pt/PPy-$C_{35\%}$ was chosen as the best electrocatalyst material for application as anode, as cathode, or as both anode and cathode of direct borohydride-peroxide fuel cells.

Acknowledgements

The authors would like to thank to the Ministry of Education, Science and Technological Development of the Republic of Serbia for support within projects no. OI172043 and III45014. The authors would also like to thank Fundação para a Ciência e a Tecnologia (FCT,

Table 7
Data summary of DBPFCs employing carbon-supported Pt-based electrocatalysts and polymer-based electrocatalysts.

Anode catalyst (loading)	Cathode catalyst (loading)	Separator	Fuel	Oxidant	T/ºC	P_{max}/mW cm^{-2}	j_{max}/mA cm^{-2}	ΔE_{max}/V	OCV/V	Ref.
Pt on carbon black (0.5 mg_{Pt} cm^{-2})	Pt/CB (0.5 mg_{Pt} cm^{-2})	Nafion117	0.1 M $NaBH_4$ + 6 M NaOH	0.1 M H_2O_2	RT	15	18	0.84	2.07	[62]
Pt on bulk polypyrrole film (0.5 mg_{Pt} cm^{-2})	Pt/BPPy (0.5 mg_{Pt} cm^{-2})	Nafion117	0.1 M $NaBH_4$ + 6 M NaOH	0.1 M H_2O_2	RT	27	42	0.67	2.07	[62]
Pt on multilayer macro/mesoporous PPy film (0.5 mg_{Pt} cm^{-2})	Pt/PPy (0.5 mg_{Pt} cm^{-2})	Nafion117	0.1 M $NaBH_4$ + 6 M NaOH	0.1 M H_2O_2	RT	56	77	0.73	2.07	[62]
Pt/C (0.9 mg_{Pt} cm^{-2})	Pt/C (0.9 mg_{Pt} cm^{-2})	Nafion117	1 M $NaBH_4$ + 3 M NaOH	2 M H_2O_2 + 0.5 H_2SO_4	RT	42.8	39.6	1.09	1.71	[93]
Pt/MWCNTs (1 mg cm^{-2})	Au	Nafion212	5 wt.% $NaBH_4$ + 10 wt.% NaOH	5 wt.% H_2O_2 + 5 wt.% H_2PO_4	RT	135.5	201	0.69	1.60	[48]
Pd	Pt/MWCNTs (1 mg cm^{-2})	Nafion212	5 wt.% $NaBH_4$ + 10 wt.% NaOH	5 wt.% H_2O_2 + 5 wt.% H_2PO_4	RT	118.6	199	0.58	1.80	[48]
PEDOT coated on graphite paper	Bare graphite paper	Fumsep FKB	1 M $NaBH_4$ + 4 M KOH	5 M H_2O_2 + 0.75 M H_2SO_4	RT	0.65	6.7	0.15	1.18	[10]
PEDOT coated on graphite paper	PEDOT coated on graphite paper	Fumsep FKB	1 M $NaBH_4$ + 4 M KOH	5 M H_2O_2 + 0.75 M H_2SO_4	RT	7.5	14.2	0.61	1.61	[10]
$Pt_{50}Co_{50}$/C (0.9 mg_{PtCo} cm^{-2})	Pt/C (0.9 mg_{Pt} cm^{-2})	Nafion117	1 M $NaBH_4$ + 3 M NaOH	2 M H_2O_2 + 0.5 M H_2SO_4	25	64.1	70	0.91	1.71	[94]
$Pt_{67}Co_{33}$/C (0.9 mg_{PtCo} cm^{-2})	Pt/C (0.9 mg_{Pt} cm^{-2})	Nafion117	1 M $NaBH_4$ + 3 M NaOH	2 M H_2O_2 + 0.5 M H_2SO_4	25	79.7	95	0.85	1.74	[94]
$Pt_{75}Co_{25}$/C (0.9 mg_{PtCo} cm^{-2})	Pt/C (0.9 mg_{Pt} cm^{-2})	Nafion117	1 M $NaBH_4$ + 3 M NaOH	2 M H_2O_2 + 0.5 M H_2SO_4	25	68.7	79.6	0.87	1.76	[94]
PtNi/C (1 mg_{PtNi} cm^{-2})	Pt/C (0.5 mg_{Pt} cm^{-2})	Nafion117	1.5 M $NaBH_4$ + 2 M NaOH	2 M H_2O_2 + 0.5 M H_2SO_4	25	68	72	0.90	1.71	[95]
PtNi/C (1 mg_{PtNi} cm^{-2})	Pt/C (0.5 mg_{Pt} cm^{-2})	Nafion117	1.5 M $NaBH_4$ + 2 M NaOH	2 M H_2O_2 + 0.5 M H_2SO_4	45	104.5	96	1.09	1.71	[95]
PtNi/C (1 mg_{PtNi} cm^{-2})	Pt/C (0.5 mg_{Pt} cm^{-2})	Nafion117	1 M $NaBH_4$ + 2 M NaOH	2 M H_2O_2 + 0.5 M H_2SO_4	45	96.8	100	0.98	1.69	[95]
PtNi/C (1 mg_{PtNi} cm^{-2})	Pt/C (0.5 mg_{Pt} cm^{-2})	Nafion117	1.5 M $NaBH_4$ + 2 M NaOH	2 M H_2O_2 + 0.5 M H_2SO_4	55	140	143	0.96	1.73	[96]
PtNi/C (1 mg cm^{-2})	Pt/C (0.5 mg cm^{-2})	Nafion117	1 M $NaBH_4$ + 2 M NaOH	2 M H_2O_2 + 0.5 M H_2SO_4	60	106.6	121.5	0.85	1.77	[96]
PtNi/C (1 mg cm^{-2})	Pt/C (0.5 mg cm^{-2})	Nafion117	2 M $NaBH_4$ + 2 M NaOH	2 M H_2O_2 + 0.5 M H_2SO_4	60	98.5	119	0.8	1.77	[96]

Portugal) for postdoctoral research grant no. SFRH/BPD/77768/2011 (B. Šljukić), for contract no. IF/01084/2014/CP1214/CT0003 under IF2014 Programme (D.M.F. Santos) and for a research grant in the associated IF2014 project (R.C.P. Oliveira). They are grateful to East Anatolia High Technology Research Center (DAYTAM) of Atatürk University for helping with ICP-MS, FTIR, Raman and XPS analyses.

Appendix A. Supplementary data

Supplementary material related to this article can be found, in the online version, at doi:https://doi.org/10.1016/j.apcatb.2018.06.057.

References

[1] B. Šljukić, J. Milikić, D.M.F. Santos, C.A.C. Sequeira, D. Macciò, A. Saccone, Electrocatalytic performance of Pt-Dy alloys for direct borohydride fuel cells, J. Power Sources 272 (2014) 335–343.
[2] J. Milikić, G. Cirić-Marjanović, S. Mentus, D.M.F. Santos, C.A.C. Sequeira, B. Šljukić, Pd/c-PANI electrocatalysts for direct borohydride fuel cells, Electrochim. Acta 213 (2016) 298–305.
[3] B. Šljukić, J. Milikić, D.M.F. Santos, C.A.C. Sequeira, Carbon-supported $Pt_{0.75}M_{0.25}$ (M = Ni or Co) electrocatalysts for borohydride oxidation, Electrochim. Acta 107 (2013) 577–583.
[4] J.H. Wee, Which type of fuel cell is more competitive for portable application: direct methanol fuel cells or direct borohydride fuel cells? J. Power Sources 161 (2006) 1–10.
[5] A.M. Pasqualeti, P.-Y. Olu, M. Chatenet, F.H.B. Lima, Borohydride electrooxidation on carbon-supported noble metal nanoparticles: insights into hydrogen and hydroxyborane formation, ACS Catal. 5 (2015) 2778–2787.
[6] P.-Y. Olu, A. Bonnefont, G. Braesch, V. Martin, E.R. Savinova, M. Chatenet, Influence of the concentration of borohydride towards hydrogen production and escape for borohydride oxidation reaction on Pt and Au electrodes – experimental and modelling insights, J. Power Sources 375 (2018) 300–309.
[7] M.G. Hosseini, R. Mahmoodi, Improvement of energy conversion efficiency and power generation in direct borohydride-hydrogen peroxide fuel cell: the effect of Ni-M core-shell nanoparticles (M = Pt, Pd, Ru)/Multiwalled Carbon Nanotubes on the cell performance, J. Power Sources 370 (2017) 87–97.
[8] V. Briega-Martos, E. Herrero, J.M. Feliu, Borohydride electro-oxidation on Pt single crystal electrodes, Electrochem. Commun. 51 (2015) 144–147.
[9] P. He, X. Wang, Y. Liu, X. Liu, L. Yi, Comparison of electrocatalytic activity of carbon-supported Au–M (M = Fe, Co, Ni, Cu and Zn) bimetallic nanoparticles for direct borohydride fuel cells, Int. J. Hydrogen Energy 37 (2012) 11984–11993.
[10] B. Bayatsarmadi, A. Peters, P. Talemi, Catalytic polymeric electrodes for direct borohydride fuel cells, J. Power Sources 322 (2016) 26–30.
[11] F.H.B. Lima, A.M. Pasqualeti, M.B. Molina Concha, M. Chatenet, E.A. Ticianelli, Borohydride electrooxidation on Au and Pt electrodes, Electrochim. Acta 84 (2012) 202–212.
[12] P.-Y. Olu, N. Job, M. Chatenet, Evaluation of anode (electro)catalytic materials for the direct borohydride fuel cell: methods and benchmarks, J. Power Sources 327 (2016) 235–257.
[13] D.M.F. Santos, B. Šljukić, L. Amaral, J. Milikić, C.A.C. Sequeira, D. Macciò, A. Saccone, Nickel-rare earth electrodes for sodium borohydride electrooxidation, Electrochim. Acta 190 (2016) 1050–1056.
[14] I. Stoševski, J. Krstić, J. Milikić, B. Šljukić, Z. Kačarević-Popović, S. Mentus, Š. Miljanić, Radiolitically synthesized nano Ag/C catalysts for oxygen reduction and borohydride oxidation reactions in alkaline media, for potential applications in fuel cells, Energy 101 (2016) 79–90.
[15] P.Y. Olu, C.R. Barros, N. Job, M. Chatenet, Electrooxidation of $NaBH_4$ in alkaline medium on well-defined Pt nanoparticles deposited onto flat glassy carbon substrate: evaluation of the effects of Pt nanoparticle size, inter-particle distance, and loading, Electrocatalysis 5 (2014) 288–300.
[16] M. Chatenet, F.H.B. Lima, E.A. Ticianelli, Gold is not a faradaic-efficient borohydride oxidation electrocatalyst: an online electrochemical mass spectrometry study, J. Electrochem. Soc. 157 (2010) B697–B704.
[17] E.G. Machado, E. Sitta, F.H.B. De Lima, J. Lee, H. Varela, Open circuit interaction of borohydride with oxidized platinum surfaces, Electrochem. Commun. 16 (2012) 107–109.
[18] D.M.F. Santos, C.A.C. Sequeira, Cyclic voltammetry investigation of borohydride oxidation at a gold electrode, Electrochim. Acta 55 (2010) 6775–6781.
[19] P.-Y. Olu, A. Bonnefont, M. Rouhet, S. Bozdech, N. Job, M. Chatenet, E. Savinova, Insights into the potential dependence of the borohydride electrooxidation reaction mechanism on platinum nanoparticles supported on ordered carbon nanomaterials, Electrochim. Acta 179 (2015) 637–646.
[20] M.G. Hosseini, N. Rashidi, R. Mahmoodi, M. Omer, Preparation of Pt/G and PtNi/G nanocatalysts with high electrocatalytic activity for borohydride oxidation and investigation of different operation condition on the performance of direct borohydride-hydrogen peroxide fuel cell, Mater. Chem. Phys. 208 (2018) 207–219.
[21] P.-Y. Olu, F. Deschamps, G. Caldarella, M. Chatenet, N. Job, Investigation of platinum and palladium as potential anodic catalysts for direct borohydride and ammonia borane fuel cells, J. Power Sources 297 (2015) 492–503.
[22] G. Braesch, A. Bonnefont, V. Martin, E.R. Savinova, M. Chatenet, Borohydride

oxidation reaction mechanisms and poisoning effects on Au, Pt and Pd bulk electrodes: from model (low) to direct borohydride fuel cell operating (high) concentrations, Electrochim. Acta 273 (2018) 483–494.
[23] M.G. Hosseini, R. Mahmoodi, Ni@M (M = Pt, Pd and Ru) core@shell nanoparticles on a Vulcan XC-72R support with superior catalytic activity toward borohydride oxidation: electrochemical and fuel cell studies, New J. Chem. 41 (2017) 13408–13417.
[24] D.S.P. Cardoso, D.M.F. Santos, B. Šljukić, C.A.C. Sequeira, D. Macciò, A. Saccone, Platinum-rare earth cathodes for direct borohydride-peroxide fuel cells, J. Power Sources 307 (2016) 251–258.
[25] P. Landon, P.J. Collier, A.J. Papworth, J. Kiely, J. Graham, Direct formation of hydrogen peroxide from H_2/O_2 using a gold catalyst, Chem. Commun. (2002) 2058–2059.
[26] L. An, C.Y. Jung, Transport phenomena in direct borohydride fuel cells, Appl. Energy 205 (2017) 1270–1282.
[27] W. Yang, S. Yang, W. Sun, G. Sun, Q. Xin, Nanostructured palladium-silver coated nickel foam cathode for magnesium-hydrogen peroxide fuel cells, Electrochim. Acta 52 (2006) 9–14.
[28] G.H. Miley, N. Luo, J. Mather, R. Burton, G. Hawkins, L. Gu, E. Byrd, R. Gimlin, P.J. Shrestha, G. Benavides, J. Laystrom, D. Carroll, Direct $NaBH_4/H_2O_2$ fuel cells, J. Power Sources 165 (2007) 509–516.
[29] N.A. Choudhury, R.K. Raman, S. Sampath, A.K. Shukla, An alkaline direct borohydride fuel cell with hydrogen peroxide as oxidant, J. Power Sources 143 (2005) 1–8.
[30] D. Cao, L. Sun, G. Wang, Y. Lv, M. Zhang, Kinetics of hydrogen peroxide electroreduction on Pd nanoparticles in acidic medium, J. Electroanal. Chem. 621 (2008) 31–37.
[31] B.D. Adams, C.K. Ostrom, A. Chen, Highly active PdPt catalysts for the electrochemical reduction of H_2O_2, J. Electrochem. Soc. 158 (2011) B434–B439.
[32] K. Doblhofer, G. Flätgen, S. Horswell, B. Pettinger, S. Wasle, K.G. Weil, Autocatalysis by the intermediate surface hydroxide formed during hydrogen peroxide reduction on silver electrodes, Surf. Sci. 603 (2009) 1900–1903.
[33] L. Gu, N. Luo, G.H. Miley, Cathode electrocatalyst selection and deposition for a direct borohydride/hydrogen peroxide fuel cell, J. Power Sources 173 (2007) 77–85.
[34] G. Selvarani, S.K. Prashant, A.K. Sahu, P. Sridhar, S. Pitchumani, A.K. Shukla, A direct borohydride fuel cell employing Prussian Blue as mediated electron-transfer hydrogen peroxide reduction catalyst, J. Power Sources 178 (2008) 86–91.
[35] K.L. Stewart, A.A. Gewirth, Mechanism of electrochemical reduction of hydrogen peroxide on copper in acidic sulfate solutions, Langmuir 23 (2007) 9911–9918.
[36] J. Ma, N.A. Choudhury, Y. Sahai, A comprehensive review of direct borohydride fuel cells, Renew. Sustain. Energy Rev. 14 (2010) 183–199.
[37] A.L. Morais, J.R.C. Salgado, B. Šljukić, D.M.F. Santos, C.A.C. Sequeira, Electrochemical behaviour of carbon supported Pt electrocatalysts for H_2O_2 reduction, Int. J. Hydrogen Energy 37 (2012) 14143–14151.
[38] S. Shahgaldi, J. Hamelin, Improved carbon nanostructures as a novel catalyst support in the cathode side of PEMFC: a critical review, Carbon 94 (2015) 705–728.
[39] E. Antolini, Carbon supports for low-temperature fuel cell catalysts, Appl. Catal. B 88 (2009) 1–24.
[40] R.C.P. Oliveira, M. Vasić, D.M.F. Santos, B. Babić, R. Hercigonja, C.A.C. Sequeira, B. Šljukić, Performance assessment of a direct borohydride-peroxide fuel cell with Pd-impregnated faujasite X zeolite as anode electrocatalyst, Electrochim. Acta 269 (2018) 517–525.
[41] M. Martins, B. Šljukić, Ö. Metin, M. Sevim, C.A.C. Sequeira, T. Şener, D.M.F. Santos, Bimetallic PdM (M = Fe, Ag, Au) alloy nanoparticles assembled on reduced graphene oxide as catalysts for direct borohydride fuel cells, J. Alloys Compd. 718 (2017) 204–214.
[42] J. Tang, J. Liu, N.L. Torad, T. Kimura, Y. Yamauchi, Tailored design of functional nanoporous carbon materials toward fuel cell applications, Nano Today 9 (2014) 305–323.
[43] M. Martins, B. Šljukić, C.A.C. Sequeira, Ö. Metin, M. Erdem, T. Şener, D.M.F. Santos, Biobased carbon-supported palladium electrocatalysts for borohydride fuel cells, Int. J. Hydrogen Energy 41 (2016) 10914–10922.
[44] I.J. García-Rosado, J. Uribe-Calderón, N. Alonso-Vante, Nitrogen-doped reduced graphite oxide as a support for CoSe electrocatalyst for oxygen reduction reaction in alkaline media, J. Electrochem. Soc. 164 (2017) F658–F666.
[45] T. Tesfu-Zeru, M. Sakthivel, J.-F. Drillet, Investigation of mesoporous carbon hollow spheres as catalyst support in DMFC cathode, Appl. Catal. B 204 (2017) 173–184.
[46] S.H. Joo, C. Pak, D.J. You, S.-A. Lee, H.I. Lee, J.M. Kim, H. Chang, D. Seung, Ordered mesoporous carbons (OMC) as supports of electrocatalysts for direct methanol fuel cells (DMFC): effect of carbon precursors of OMC on DMFC performances, Electrochim. Acta 52 (2006) 1618–1626.
[47] R. Zolfaghari, F. Ahmadun, M.R. Othman, W.R.W. Daud, M. Ismail, Nonionic surfactant-templated mesoporous carbon as an electrocatalyst support for methanol oxidation, Mater. Chem. Phys. 139 (2013) 262–269.
[48] T.H. Oh, B. Jang, S. Kwon, Electrocatalysts supported on multiwalled carbon nanotubes for direct borohydride–hydrogen peroxide fuel cell, Int. J. Hydrogen Energy 39 (2014) 6977–6986.
[49] J.Q. Yang, B.H. Liu, S. Wu, Carbon-supported Pd catalysts: influences of nanostructure on their catalytic performances for borohydride electrochemical oxidation, J. Power Sources 194 (2009) 824–829.
[50] Y. Zhou, S. Li, Y. Chen, Y. Liu, The high utilization of fuel in direct borohydride fuel cells with a $PdNi_x$-B/carbon nanotubes-catalysed anode, J. Power Sources 351 (2017) 79–85.
[51] P.Y. You, S.K. Kamarudin, Recent progress of carbonaceous materials in fuel cell applications: an overview, Chem. Eng. J. 309 (2017) 489–502.
[52] M. Liu, R. Zhang, W. Chen, Graphene-supported nanoelectrocatalysts for fuel cells: synthesis, properties, and applications, Chem. Rev. 114 (2014) 5117–5160.
[53] R. Valiollahi, R. Ojani, Pt hollow nanospheres/graphene electrocatalytic ability toward sodium borohydride oxidation: a study of morphology effect on electrocatalytic activity, J. Appl. Electrochem. 47 (2017) 205–212.
[54] L. Borchardt, Q.-L. Zhu, M.E. Casco, R. Berger, X. Zhuang, S. Kaskel, X. Feng, Q. Xu, Toward a molecular design of porous carbon materials, Mater. Today 20 (2017) 592–610.
[55] Y.-J. Wang, B. Fang, H. Li, X.T. Bi, H. Wang, Progress in modified carbon support materials for Pt and Pt-alloy cathode catalysts in polymer electrolyte membrane fuel cells, Prog. Mater. Sci. 82 (2016) 445–498.
[56] E. Antolini, Composite materials for polymer electrolyte membrane microbial fuel cells, Biosens. Bioelectron. 69 (2015) 54–70.
[57] H. Zhao, L. Li, J. Yang, Y. Zhang, H. Li, Synthesis and characterization of bimetallic Pt-Fe/polypyrrole-carbon catalyst as DMFC anode catalyst, Electrochem. Commun. 10 (2008) 876–879.
[58] F. Xu, C. Innocent, B. Bonnet, D.J. Jones, J. Rozière, Chemical modification of perfluorosulfonated membranes with pyrrole for fuel cell application: preparation, characterisation and methanol transport, Fuel Cells 5 (2005) 398–405.
[59] A.K. Sharma, J. Kim, Y. Lee, An efficient synthesis of polypyrrole/carbon fiber composite nano-thin films, Int. J. Electrochem. Sci. 4 (2009) 1560–1567.
[60] F. Bensebaa, A.A. Farah, D. Wang, C. Bock, X. Du, J. Kung, Y. Le Page, Microwave synthesis of polymer-embedded Pt-Ru catalyst for direct methanol fuel cell, J. Phys. Chem. B 109 (2005) 15339–15344.
[61] E. Das, A.B. Yurtcan, Effect of carbon ratio in the polypyrrole/carbon composite catalyst support on PEM fuel cell performance, Int. J. Hydrogen Energy 41 (30) (2016) 13171–13179.
[62] K. Sombatmankhong, Improved performance and stability of direct borohydride fuel cells (DBFCs) with porous polypyrrole support, J. Porous Mater. 22 (2015) 675–687.
[63] F. Memioğlu, A. Bayrakçeken, T. Öznülüer, M. Ak, Synthesis and characterization of polypyrrole/carbon composite as a catalyst support for fuel cell applications, Int. J. Hydrogen Energy 37 (2012) 16673–16679.
[64] E. Daş, A.B. Yurtcan, PEDOT/C Composites used as a proton exchange membrane fuel cell catalyst support: role of carbon amount, Energy Technol. 5 (2017) 1552–1560.
[65] D.M.F. Santos, C.A.C. Sequeira, Effect of membrane separators on the performance of direct borohydride fuel cells, J. Electrochem. Soc. 159 (2012) B126–B132.
[66] D.M.F. Santos, P.G. Saturnino, R.F.M. Lobo, C.A.C. Sequeira, Direct borohydride/peroxide fuel cells using Prussian Blue cathodes, J. Power Sources 208 (2012) 131–137.
[67] S. Mokrane, L. Makhloufi, N. Alonso-Vante, Electrochemistry of platinum nanoparticles supported in polypyrrole (PPy)/C composite materials, J. Solid State Electrochem. 12 (2008) 569–574.
[68] S. Konwer, S.K. Dolui, Synthesis and characterization of polypyrrole/graphite composites and study of their electrical and electrochemical properties, Mater. Chem. Phys. 124 (2010) 738–743.
[69] L. Bokobza, J.-L. Bruneel, M. Couzi, Raman spectroscopy as a tool for the analysis of carbon-based materials (highly oriented pyrolitic graphite, multilayer graphene and multiwall carbon nanotubes) and of some of their elastomeric composites, Vib. Spectrosc. 74 (2014) 57–63.
[70] L. Bokobza, J.-L. Bruneel, M. Couzi, Raman spectra of carbon-based materials (from graphite to carbon black) and of some silicone composites, J. Carbon Res. 1 (2015) 77–94.
[71] Q. Zhao, H.D. Wagner, Raman spectroscopy of carbon-nanotube-based composites, Philos. Trans. R. Soc. Lond. A 362 (2004) 2407–2424.
[72] L. Castanheira, L. Dubau, M. Mermoux, G. Berthomé, N. Caqué, E. Rossinot, M. Chatenet, F. Maillard, Carbon corrosion in proton-exchange membrane fuel cells: from model experiments to real-life operation in membrane electrode assemblies, ACS Catal. 4 (2014) 2258–2267.
[73] L. Castanheira, W.O. Silva, F.H.B. Lima, A. Crisci, L. Dubau, F. Maillard, Carbon corrosion in proton-exchange membrane fuel cells: effect of the carbon structure, the degradation protocol, and the gas atmosphere, ACS Catal. 5 (2015) 2184–2194.
[74] L. Wang, F. Liu, C. Jin, T. Zhang, Q. Yin, Preparation of polypyrrole/graphene nanosheets composites with enhanced thermoelectric properties, RSC Adv. 4 (2014) 46187–46193.
[75] Y. Ren, J. Zhang, Q. Xu, Z. Chen, D. Yang, B. Wang, J. Zheng, Biomass-derived three-dimensional porous N-doped carbonaceous aerogel for efficient supercapacitor electrodes, RSC Adv. 4 (2014) 23412–23419.
[76] M.S. Dresselhaus, A. Jorio, A.G. Souza Filho, R. Saito, Defect characterization in graphene and carbon nanotubes using Raman spectroscopy, Philos. Trans. R. Soc. A 368 (2010) 5355–5377.
[77] L.G. Cançado, M.G. da Silva, E.H.M. Ferreira, F. Hof, K. Kampioti, K. Huang, A. Pénicaud, C.A. Achete, R.B. Capaz, A. Jorio, Disentangling contributions of point and line defects in the Raman spectra of graphene-related materials, 2D Mater. 4 (2017) 025039.
[78] Y. Chen, Y. Li, H. Wang, M. Yang, Gas sensitivity of a composite of multi-walled carbon nanotubes and polypyrrole prepared by vapor phase polymerization, Carbon 45 (2007) 357–363.
[79] T.N. Tran, M.Y. Song, K.P. Singh, D.S. Yang, J.S. Yu, Iron-polypyrrole electrocatalysts with remarkable activity and stability for ORR in both alkaline and acidic conditions: a comprehensive assessment of catalyst preparation sequence, J. Mater. Chem. A 4 (2016) 8645–8657.
[80] M.R. Karim, C.J. Lee, A.M.S. Chowdhury, N. Nahar, M.S. Lee, Radiolytic synthesis of conducting polypyrrole/carbon nanotube composites, Mater. Lett. 61 (2007) 1688–1692.

[81] E. Gyenge, M. Atwan, D. Northwood, Electrocatalysis of borohydride oxidation on colloidal Pt and Pt-alloys (Pt-Ir, Pt-Ni, and Pt-Au) and application for direct borohydride fuel cell anodes, J. Electrochem. Soc. 153 (2006) A150–A158.
[82] J.I. Martins, M.C. Nunes, R. Koch, L. Martins, M. Bazzaoui, Electrochemical oxidation of borohydride on platinum electrodes: the influence of thiourea in direct fuel cells, Electrochim. Acta 52 (2007) 6443–6449.
[83] Z. Jusys, R.J. Behm, Borohydride electrooxidation over Pt/C, AuPt/C and Au/C catalysts: partial reaction pathways and mixed potential formation, Electrochem. Commun. 60 (2015) 9–12.
[84] A.J. Bard, L.R. Faulkner, Electrochemical Methods: Fundamentals and Applications, 2nd edition, John Wiley & Sons, Inc., Texas, United States, 2001.
[85] D.M.F. Santos, P.G. Saturnino, D. Macciò, A. Saccone, C.A.C. Sequeira, Platinum-rare earth intermetallic alloys as anode electrocatalysts for borohydride oxidation, Catal. Today 170 (2011) 134–140.
[86] J.P. Elder, A. Hickling, Anodic behaviour of the borohydride ion, Trans. Faraday Soc. 58 (1962) 1852–1864.
[87] E. Gyenge, Electrooxidation of borohydride on platinum and gold electrodes: implications for direct borohydride fuel cells, Electrochim. Acta 49 (2004) 965–978.
[88] A. Tegou, S. Papadimitriou, I. Mintsouli, S. Armyanov, E. Valova, G. Kokkinidis, S. Sotiropoulos, Rotating disc electrode studies of borohydride oxidation at Pt and bimetallic Pt-Ni and Pt-Co electrodes, Catal. Today 170 (2011) 126–133.
[89] H. Cheng, K. Scott, Determination of kinetic parameters for borohydride oxidation on a rotating Au disk electrode, Electrochim. Acta 51 (2006) 3429–3433.
[90] D.A. Finkelstein, C.D. Letcher, D.J. Jones, L.M. Sandberg, D.J. Watts, H.D. Abruña, Self-poisoning during BH_4– oxidation at Pt and Au, and in situ poison removal procedures for BH_4– fuel cells, J. Phys. Chem. C 117 (2013) 1571–1581.
[91] D.M. Liu, W.J. Huang, T.Z. Si, Q.A. Zhang, Hydrogen storage properties of $LiBH_4$ destabilized by SrH_2, J. Alloys Compd. 551 (2013) 8–11.
[92] D.M.F. Santos, D.S.P. Cardoso, B. Šljukić, C.A.C. Sequeira, D. Macciò, A. Saccone, Nickel-rare earth (RE = Ce, Sm, Dy) electrodes for H_2O_2 reduction in fuel cells, ECS Trans. 72 (2016) 31–40.
[93] L. Yi, W. Wei, C. Zhao, C. Yang, L. Tian, J. Liu, X. Wang, Electrochemical oxidation of sodium borohydride on carbon supported Pt-Zn nanoparticle bimetallic catalyst and its implications to direct borohydride-hydrogen peroxide fuel cell, Electrochim. Acta 158 (2015) 209–218.
[94] L. Yi, L. Liu, X. Liu, X. Wang, W. Yi, P. He, X. Wang, Carbon-supported Pt-Co nanoparticles as anode catalyst for direct borohydride-hydrogen peroxide fuel cell: electrocatalysis and fuel cell performance, Int. J. Hydrogen Energy 37 (2012) 12650–12658.
[95] M. Abdolmaleki, M.G. Hosseini, A development in direct borohydride/hydrogen peroxide fuel cell using nanostructured Ni-Pt/C anode, Fuel Cells 17 (2017) 321–327.
[96] M.G. Hosseini, R. Mahmoodi, M.S. Amjadi, Carbon supported Ni_1Pt_1 nanocatalyst as superior electrocatalyst with increased power density in direct borohydride-hydrogen peroxide and investigation of cell impedance at different temperatures and discharging currents, Energy 131 (2017) 137–148.
[97] X. Wang, W. Wei, L. Jing, Q. Zhao, S. Chen, L. Yi, X. Wang, W. Wei, Nanoporous carbon supported platinum-copper nanocomposites as anode catalysts for direct borohydride-hydrogen peroxide fuel cell, Electrochim. Acta 171 (2015) 96–104.
[98] H.Y. Qin, Z.X. Liu, L.Q. Ye, J.K. Zhu, Z.P. Li, The use of polypyrrole modified carbon-supported cobalt hydroxide as cathode and anode catalysts for the direct borohydride fuel cell, J. Power Sources 192 (2009) 385–390.